THE JOURNAL OF PHYSICAL CHEMISTRY C

Article

pubs.acs.org/JPCC

Investigation of the Mechanisms Giving Rise to TADF in Exciplex States

Paloma L. dos Santos, Fernando B. Dias, and Andrew P. Monkman*

OEM Research Group, Physics Department, Durham University, South Road, Durham DH1 3LE, United Kingdom

Supporting Information

ABSTRACT: The donor–acceptor systems studied in this work have been demonstrated to show strong exciplex formation by their red-shifted PL emission when compared with the individual donor and acceptor molecules, and all give rise to delayed fluorescence. In all cases, the channels by which this delayed fluorescence is generated, along with the energy levels involved in reverse intersystem crossing (rISC), that is, which triplet levels the charge-transfer states couple to yield spin flip, have not previously been identified. Here the intermolecular charge transfer states formed in the donor–acceptor molecular pairs are studied. It is demonstrated that the local triplet excited states are the states that couple to the singlet charge-transfer excited state, defining the rISC process and hence thermally activated delayed fluorescence (TADF) mechanism. Moreover, in most systems there is a competition between delayed fluorescence mechanisms, triplet triplet annihilation and TADF, and this is analysed in detail. New design rules for exciplex materials showing dominant delayed fluorescence due to rISC for the device based on TADF are elucidated.

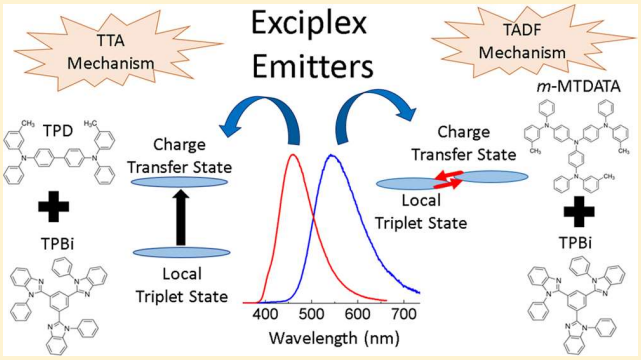

INTRODUCTION

Exciplex formation in organic materials, which are intermolecular charge transfer (iMCT) states between electron donor (**D**) and acceptor (**A**) molecules, that is, an excited-state complex between the donor and acceptor molecules, and their application in organic light-emitting diodes (OLEDs) have attracted significant attention due to the observation of thermally activated delayed fluorescence (TADF) in some examples.[1−4] Exciplex formation has for a long time been regarded as a negative effect in OLEDs due to reducing device performances, damaging color purity, especially when they form interfacial states between the transport and the emissive layers in devices.[5,6] However, when exciplex emitters are used as emissive layers in devices, they can show great performance because of the capability they offer to harvest lower energy triplet excitons (otherwise dark states) into emissive singlet states of higher energy, thereby surpassing the natural 25% internal quantum efficiency limit. Up-conversion of triplet excitons to singlet states can be achieved mainly by two different mechanisms: triplet–triplet annihilation (TTA) and thermally activated delayed fluorescence (TADF). In TTA, the theoretical maximum internal quantum efficiency a device could achieve is 62.5%, whereas in TADF this efficiency can theoretically achieve 100%.[7] Hence, emitters that show the latter mechanism are very attractive for OLEDs applications.

The key to engineering an efficient TADF emitter is to achieve a small energy splitting between the lowest energy singlet and triplet states (exchange energy) within the molecular complex, and the exciplex systems are promising candidates to show this characteristic.[8] These molecular systems can have small exchange energy because electrons and holes are located on two different molecules, leading to very small spatial wave function overlap and hence small exchange energy, and hence singlet triplet energy splitting (ΔE_{ST}) will be small. However, the number of available exciplex emitters showing a true TADF mechanism is still limited, and strategies for designing exciplexes with this character are greatly desirable because, presently, the only "design" rule for an exciplex to yield TADF is that there should not be a low-lying local triplet state that quenches all excited states.[9]

Intersystem crossing between the charge-transfer singlet (^{1}CT) and charge-transfer triplet (^{3}CT) states in a **D-A** molecules is very inefficient compared with that between a ^{1}CT state and a locally excited triplet state (^{3}LE) of the **D** or **A** molecule. This is due to the lack of changing the spatial orbital angular momentum that is associated with electronic transition between ^{1}CT and ^{3}CT. Hence, the spin of the ^{1}CT state can only couple strongly to a close in energy ^{3}LE state.[10−12] The spin flip mechanism and decay to the ^{3}LE state is not described by simple processes obeying El-Sayed's rules. This is shown in the work of Chen et al. and Marian.[12,13] Moreover, from our recent quantum-chemical calculations, the process is found to be a second-order mechanism mediated by vibronic coupling between the ^{3}LE and ^{3}CT states to allow spin-orbit coupling

Received: May 23, 2016
Revised: July 26, 2016

ACS Publications © XXXX American Chemical Society

DOI: 10.1021/acs.jpcc.6b05198
J. Phys. Chem. C XXXX, XXX, XXX−XXX

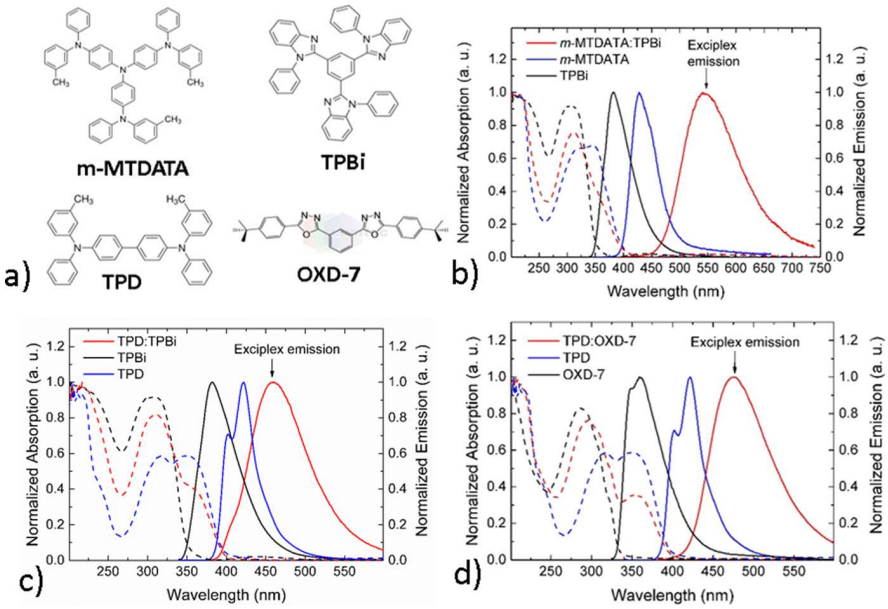

Figure 1. (a) Chemical structure of *m*-MTDATA, TPBi, TPD, and OXD-7. Normalized photoluminescence (PL) and absorption spectra of (b) *m*-MTDATA:TPBi, (c) TPD:TPBi, and (d) TPD:OXD-7 as well as their pristine acceptor and donor molecules.

(SOC) back to the ^{1}CT.[14] This vibronic coupling mechanism also gives rise to the intersystem crossing (ISC) from ^{1}CT to ^{3}LE. It is clear that without the vibronic coupling between ^{3}LE and ^{3}CT both ISC and rISC will be at least six orders of magnitude too slow as compared with the measured ISC and rISC rates in intramolecular D−A systems. Therefore, the common believe that the harvesting of triplet states occurs between ^{3}CT triplet and ^{1}CT singlet states is not correct. We have recently reported that the ^{3}LE of the **D** or **A** units is the essential triplet state controlling the ΔE_{ST} energy and reverse intersystem crossing (rISC) in intramolecular charge transfer (ICT) TADF emitters, the **D**-**A**-**D** butterfly-shaped molecules.[15,16] In the case of an exciplex, the comparison between exciplex and ICT systems seems difficult; however, one needs to consider that two different factors control SOC: (i) the overlap of the wave functions of the two electrons in the exciplex state and (ii) the electronic coupling between them, which falls off as $1/r^3$.[17,18] One way to view SOC is the spin interaction of one electron's angular momentum in the magnetic field of the other orbiting electron, which quantum mechanically follows the exchange interaction between the two electrons and falls off very quickly with increasing electron separation, typically at 1.5 nm separation the SOC rate $<10^0$ s^{-1}.[19] Thus, the exact orientation of **D** and **A** molecules in an exciplex does not affect SOC rates as it does in ICT systems because the exchange interaction is already very small because the electron separation distance is >1 nm; SOC is totally dominated by the electron separation spatial term. In an intermolecular exciplex system, the electron separation is large,[20] showing exciplex separations in the range 2 to 3 nm, with the separation and intensity controlled by external electric field. Thus no SOC will occur between ^{1}CT and ^{3}CT irrespective of relative orientation of **D** and **A** in an exciplex; it is totally overwhelmed by the large electron separation, and a different mechanism is responsible for singlet−triplet interconversion.

Here we show that the same mechanism for SOC proposed in ICT systems[14] is valid in bimolecular exciplex emitters. By studying different blends made of well-known electron **D** and **A** materials we show by time-resolved spectroscopy that the ISC/rISC processes are mediated between ^{1}CT and local triplet states (^{3}LE). Consequently, to obtain efficient TADF exciplex emitters the ^{3}LE state from the **D** or **A** molecules should be close enough in energy to the ^{1}CT state to minimize the thermal activation barrier between them. We also analyze TTA and TADF mechanisms in exciplex blends; for those systems with small energy splitting between ^{1}CT and ^{3}LE, the TADF mechanism dominates; in contrast, TTA dominates for larger ΔE_{ST} because the residence time in ^{3}LE is long and TTA outcompetes rISC. We also analyze the role of the highest occupied and lowest unoccupied molecular orbital (HOMO/LUMO) energies levels between the electron **D** and **A** molecules in the exciplex by combining the results of a large number of exciplex systems, and we find no direct correlation between HOMO or LUMO energy offsets and TADF because of the dominance of the ^{1}CT and ^{3}LE energy difference on rISC and thus TADF.

In brief, we present important new contributions toward the full elucidation of the underlying mechanism of TADF in exciplex systems, leading to a reduction in time and cost in the development of new emitter materials to efficient OLEDs.

EXPERIMENTAL SECTION

Pure thin films and mixed blends were made of the following materials: *N*,*N*′-bis(3-methylphenyl)-*N*,*N*′-diphenylbenzidine (TPD); 1,3-bis[2-(4-*tert*-butylphenyl)-1,3,4-oxadiazo-5-yl]-benzene (OXD-7); 2,2′,2″-(1,3,5-benzinetriyl)-tris(1-phenyl-1-*H*-benzimidazole) (TPBi); 2,9-dimethyl-4,7-diphenyl-1,10-phenanthroline (BCP); tris(4-carbazoyl-9-ylphenyl)amine (TCTA); 4,4′-cyclohexylidenebis[*N*,*N*-bis(4-methylphenyl)-benzenamine] (TAPC); 2-phenyl-5-(4-biphenylyl)-1,3,4-oxadiazole (PBD), 1,3-di(9*H*-carbazol-9-yl)benzene (*m*CP); and 4,4′,4″-tris[phenyl(*m*-tolyl)amino]triphenylamine (*m*-MTDATA). All materials were purchased from Sigma-Aldrich or Lumtec and further purified using vacuum sublimation (CreaPhysics). The molecules were deposited as thin films by

DOI: 10.1021/acs.jpcc.6b05198
J. Phys. Chem. C XXXX, XXX, XXX−XXX

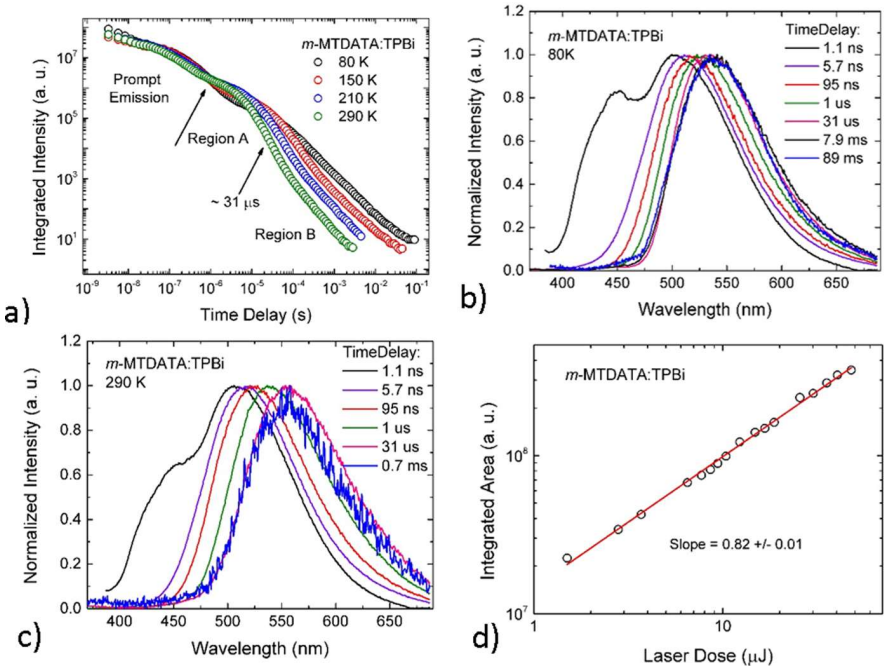

Figure 2. (a) Time-resolved fluorescence decay curves at different temperatures. Time-resolved normalized emission spectra at (b) 80 and (c) 290 K. (d) Integrated area as a function of the laser excitation (337 nm) of *m*-MTDATA:TPBi blend.

evaporation. Pure evaporated thin films and blend films (coevaporation) were deposited onto transparent sapphire substrates using a Kurt J. Lesker Spectros II deposition system under vacuum, 10^{-6} mbar. The thickness of the evaporated thin films is ~200 nm. All blends were mixed in the ratio **D**:**A** 1:1.

Steady-state absorption and emission spectra were acquired using a UV-3600 Shimadzu spectrophotometer and a Jobin Yvon Horiba Fluoromax 3, respectively. Time-resolved spectra were obtained by exciting the sample with a Nd:YAG laser (EKSPLA), 10 Hz, 355 or 266 nm or by using a Nitrogen laser, 10 Hz, 337 nm. Sample emission was directed onto a spectrograph and gated iCCD camera (Stanford Computer Optics).

RESULTS AND DISCUSSION

Figure 1a shows the chemical structure of *m*-MTDATA, TPBi, TPD, and OXD-7. Figure 1b–d shows the normalized absorption (dashed lines) and emission spectra (solid lines) for the following blends, (b) *m*-MTADATA:TPBi, (c) TPD:TPBi, and (d) TPD:OXD-7, as well as the spectra of the pristine films of donor and acceptor molecules. The films were excited by 337 or 355 nm at room temperature.

The absorption spectra of the blends show features that are nearly identical to the combination of those pristine **D** and **A** films. This result shows that the formation of a new ground-state transition does not occur in the blend films. However, their emission spectra are broader and significantly red-shifted when compared with either the **D** or **A** pristine emission spectra. These observations confirm the formation of new excited state in the blend films, that is, exciplex formation. Unambiguous exciplex emission spectra are assigned in all cases.

The exciplex formation among *m*-MTADATA:TPBi, TPD:TPBi, and TPD:OXD-7 has been reported before.[21−24] To the best of our knowledge exciplex formation was only identified and the blends were applied in OLEDs or considered as a negative effect that reduces the quality of devices without further investigation. Thus, we proceeded to investigate these exciplexes in detail by time-resolved spectroscopy.

Figure 2a shows the decay curves of *m*-MTDATA:TPBi from the early prompt emission (time delay (TD) = 1.1 ns) to the end of delayed fluorescence emission (TD = 89 ms) at different temperatures. The curves were obtained with 355 nm excitation (>200 μJ). The decay curves first show a rapid decay, associated with prompt emission, and later a long-lived emission, associated with delayed fluorescence emission. The delayed fluorescence region can be subdivided and analyzed in two different time windows, regions A and B. Initially, region A shows a temperature dependence typical for a TADF mechanism, that is, higher intensities at higher temperatures, because of the increase in thermal activation energy. However, region B, shows an unexpected behavior for a TADF mechanism; the intensity is higher for low temperatures. This behavior can be understood by analyses of the rISC rate (k_{RISC}), eq 1a,b[25]

$$k_{RISC} = k_{ISC}^{-T} e^{-\Delta E_{ST}/kT} \text{ (a)} \qquad k_{RISC} = \frac{1}{\tau_{TADF}} \frac{\int I_{TADF}(t)\,dt}{\int I_{PF}(t)\,dt} \text{ (b)} \tag{1}$$

where K_{RISC} is the rISC rate from triplet level to singlet, k_{ISC}^{-T} is the maximum rISC rate, ΔE_{ST} is the energy splitting between singlet and triplet levels, k is the Boltzmann constant, τ_{TADF} is the lifetime of the TADF component, I_{TADF} is the delayed fluorescence component, and I_{PF} the prompt fluorescence component. At high temperature, K_{RISC} is maximized (eq 1a), which leads to a short τ_{TADF} (eq 1b), giving rise to a fast decay curve. On the contrary, at low temperature, K_{RISC} and internal conversion are minimized and the triplet state will live longer, leading to a long-lived decay curve, as observed. Thus, the decay lifetime increases with decreasing temperature, as shown in Figure 2a.

DOI: 10.1021/acs.jpcc.6b05198
J. Phys. Chem. C XXXX, XXX, XXX−XXX

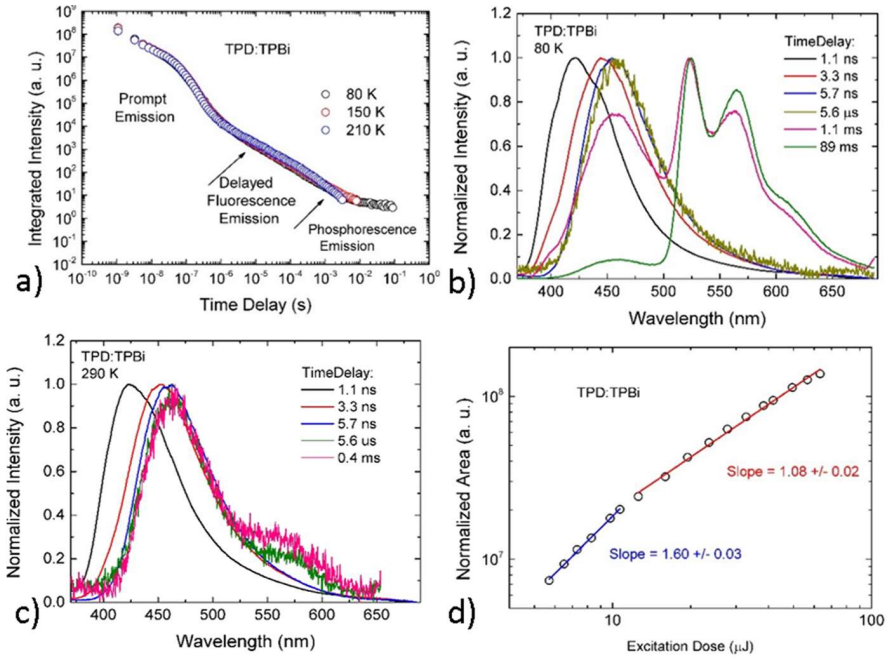

Figure 3. (a) Time-resolved fluorescence decay curves at different temperatures. Time-resolved normalized emission spectra at (b) 80 and (c) 290 K. (d) Integrated area as a function of the laser excitation (337 nm) of TPD:TPBi blend.

Figure 2b shows the analyses of the emission spectra in the entire region of the study at 80 K. At earlier times, TD = 1.1 ns, a first peak at 425 nm and the ^{1}CT state emission are observed. The first peak is associated with a vestige of the donor emission (^1LE_D), *m*-MTDATA. As the time delay increases, this peak emission disappears, showing that the process of electron transfer from the donor to the acceptor molecules has finished over ~4.6 ns, giving a rate for the electron-transfer process estimated at ca. 2×10^8 s^{-1}. During the prompt emission and region A, a continuous red shift is observed, which is associated with the energetic relaxation of the CT state. Around TD = 31 μs, the ^{1}CT state stabilizes and the same emission is observed until TD = 89 ms. The same analyses were made at 290 K, the temperature at which TADF mechanism is maximized (Figure 2c). The main difference from those spectra measured at 80 K is that the ^{1}CT is slightly further red-shifted at longer time delays. This shows that the ^{1}CT state suffers more relaxation at higher temperatures due to the increased vibrational energy.

As can be seen in Figure 2b,c, no phosphorescence emission was detected from the *m*-MTDATA:TPBi blend. Most probably, all excitons in the triplet states are efficiently converted back to ^{1}CT due to the small energy splitting between singlet and triplet states. Second-order (vibrationally coupled)[12,14] SOC allows intersystem crossing, direct, and reverse (ISC/rISC processes) to occur between the states ^{1}CT $\leftrightarrow$ ^3LE_A and ^{1}CT $\leftrightarrow$ ^3LE_D, where ^3LE_A and ^3LE_D refer to local triplet state of the acceptor and donor molecules, respectively. *m*-MTDATA:TPBi blend shows ^{1}CT energy level of (2.64 $\pm$ 0.02) eV, which was determined by the onset of the PL emission at 290 K. The phosphorescence of the pristine donor and acceptor molecules were identified, and the spectra are shown in Figure S1. The ^3LE_D has onset at (2.65 $\pm$ 0.02) eV and ^3LE_A at (2.66 $\pm$ 0.02) eV, leading to very small values of ΔE_{ST}, (−0.01 $\pm$ 0.03) and (−0.02 $\pm$ 0.03) eV, maximizing the ISC/rISC processes. The negative values mean that the ^{3}LE is located above the ^{1}CT.

The intensity dependence of the DF emission in region A (TD = 2 μs, Ti = 5 μs) was analyzed also as a function of the laser excitation dose to certify that the DF was due to a TADF mechanism and not TTA. A linear gradient of 0.82 $\pm$ 0.02 was found (Figure 2d), confirming the thermally assisted mechanism as opposed to TTA. In general, TADF complexes show slope close to 1 at low and high excitation doses, while TTA complexes show slope close to 2 at low excitation doses turning to slope close to 1 at high excitation doses.[25]

Figure 3a shows the decay curve of TPD:TPBi from the early prompt emission (TD = 1.1 ns) to the end of the PH emission (TD = 89 ms) at different temperatures (excitation at 355 nm, >200 μJ). The decay curves show first a rapid decay, associated with prompt emission, and a long-lived emission, associated with delayed fluorescence emission. Also, a very long-lived emission at low temperatures is observed associated with phosphorescence emission. There is no strong temperature dependence anywhere between 80 and 210 K, but a slight increase in the intensity of the assigned DF region is observed at higher temperatures. However, it is clear that at low temperature the emission detected lives longer.

Figure 3b shows the analyses of the emission spectra in the entire region of the study at 80 K. Initially, at early TD, the ^1LE_D emission of the **D**, TPD, is detected; then, the ^{1}CT emission spectra grows in. At TD = 5.7 ns, pure ^{1}CT emission is observed with onset at (3.05 $\pm$ 0.02) eV. The rate of electron transfer in the TPD:TPBi was estimated at ca. 2×10^8 s^{-1}. Very interestingly, at 5.7 ns only ^{1}CT emission is observed; no high-energy shoulder coming from ^1LE_D emission is seen as at earlier times, but at 1.1 ms one observes a contribution from ^1LE_D emission again. This very delayed ^1LE_D emission must come from TTA because it is the only mechanism that can regenerate a ^1LE_D state. Given that films are made by coevaporation it is very unlikely that there are large regions of segregated **D**, and hence the ^1LE_D emission most likely comes from ^1LE_D states formed by TTA, which decay radiatively before electron

DOI: 10.1021/acs.jpcc.6b05198
J. Phys. Chem. C XXXX, XXX, XXX−XXX

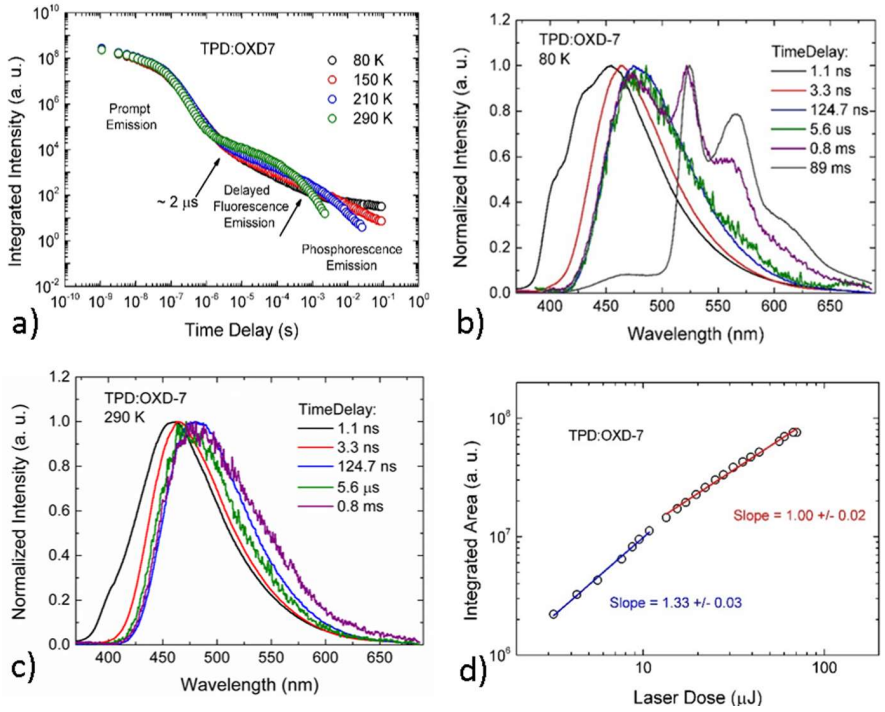

Figure 4. (a) Time-resolved fluorescence decay curves at different temperatures. Time-resolved normalized emission spectra at (b) 80 and (c) 290 K. (d) Integrated area as a function of the laser excitation (337 nm) of TPD:OXD-7.

transfer to the ^{1}CT manifold occurs. At later time, the ^{1}CT emission starts to compete with PH emission, and both emissions are observed at TD = 1.1 ms. The PH is the dominant emission at TD = 89 ms, but we still can detect a vestige of ^{1}CT emission around 450 nm. The phosphorescence emission is well-structured and show two peaks, at 523 and 564 nm, and a shoulder, at 615 nm, which matches the local triplet state emission of the **D**, TPD (^{3}LE$_D$ has onset at (2.44 ± 0.02) eV). However, the PH of TPBi, acceptor molecules, also emits in this wavelength region (onset at ^{3}LE$_A$= (2.66 ± 0.02) eV) but has different peak positions. For better comparison, the spectra of the blend TPD:TPBi and the pristine TPD and TPBi at TD = 89 ms are shown in Figure S2. Thus, the energy splitting between ^{1}CT and ^{3}LE$_D$ was found to be ΔE_{ST} = (0.61 ± 0.03) eV, and between ^{1}CT and ^{3}LE$_A$, ΔE_{ST} = (0.39 ± 0.03) eV. Both ΔE_{ST} are large, and TADF is unlikely. The spectra analyses at 290 K (Figure 2c) show that the phosphorescence emission from the ^{3}LE$_D$ is very weak, and just a shoulder is observed around 550 nm. This clearly shows that the TTA mechanism is dominating at high temperatures, and the excitons no long populate the triplet states, explaining why no emission is detected after TD = 0.4 ms.

Figure 3d shows the integrated area as a function of the laser excitation dose (337 nm), collected in the delayed fluorescence region (TD = 2 μs and Ti = 20 μs). The intensity dependence shows a slope of 1.60 ± 0.03 at low excitation dose (<11 μJ), which turns to slope of 1.08 ± 0.02 at high excitation doses. This behavior strongly indicates a dominant TTA mechanism.

Figure 4a shows the decay curves of TPD:OXD-7 from the early prompt emission (time delay (TD) = 1.1 ns) to the end of the phosphorescence (PH) emission (TD = 89 ms) at different temperatures (excitation at 355 nm, >200 μJ). There is a clear separation between prompt emission and delayed fluorescence (DF) emission around TD = 2 μs. The prompt emission does not show temperature dependence, exhibiting the same intensity from 80 K to room temperature, while the DF and PH regions show clear temperature dependence. DF emission shows higher intensity at higher temperatures, in accordance with a TADF mechanism. PH emission shows higher intensity at low temperatures, as expected from triplet emission with reduction in nonradiative decay channels.

Figure 4b shows the analyses of the emission spectra in the entire region of the study at 80 K. At earlier times, the emission spectra has two shoulders, at 403 and 426 nm, which match those of the local singlet state (^{1}LE$_D$) of the D, TPD. As the time delay increases, the emission spectra shift to longer wavelengths, moving from ^{1}LE$_D$ to ^{1}CT emission, clearly showing that the process of electron transfer from the D to the A molecules over ~2 ns at a rate of $K_{ET} \approx 5 \times 10^8$ s^{-1}, faster than those estimated for *m*-MTDATA:TPBi and TPD:TPBi. From formation until ca. TD = 124.7 ns the ^{1}CT emission is observed to relax and further red shift to an onset of (2.95 ± 0.02) eV. At later time, the ^{1}CT emission starts to compete with phosphorescence emission, and both emissions are observed at TD = 0.8 ms, for example. The phosphorescence outcompetes the ^{1}CT emission being the dominant emission at TD = 89 ms, but a vestige of ^{1}CT emission around 475 nm is still detected. The PH emission is well-structured and shows two peaks, at 526 and 569 nm, and a shoulder at 615 nm. This triplet emission originates from the localized triplet state of the donor, TPD. For better comparison, the spectra of the blend TPD:OXD-7 and the pristine TPD and OXD-7 at TD = 89 ms are shown in Figure S3. The ^{3}LE$_D$ has onset at (2.44 ± 0.02) eV. Thus, the ^{1}CT and the ^{1}LE$_D$ (lowest energy excited states) were identified in the TPD:OXD-7 blend, and the energy splitting between these two states was found to be ΔE_{ST} = (0.51 ± 0.03) eV. The ΔE_{ST} between ^{1}CT and ^{3}LE$_D$ is relatively large and unlikely for TADF to be efficient, as shown in the rISC rate equations (eq 1). However, the ^{3}LE$_A$ from the acceptor molecules, OXD-7, was identified to have onset at

DOI: 10.1021/acs.jpcc.6b05198
J. Phys. Chem. C XXXX, XXX, XXX−XXX

(2.72 ± 0.02) eV. Thus, the energy splitting between ^{1}CT and ^{3}LE$_A$ is ΔE_{ST} = (0.23 ± 0.03) eV, and rISC involving these two state would have much higher probability. Therefore, there could well be a complex competition between TTA (process involving ^{1}LE$_D$ and ^{3}LE$_D$ energy states) and TADF (process involving ^{1}CT and ^{3}LE$_A$ energy states) depending on the relative lifetime of each process.

Figure 4c shows the normalized spectra at different time delays at 290 K. As can be seen, the contribution of the donor emission at TD = 1.1 ns is higher at 80 K than at 290 K because at low temperature the nonradiative decays are minimized. Also, the ^{1}CT is slightly red shifted at longer time delays because at higher temperatures the environment has more vibrations, leading to more relaxation of ^{1}CT state.

The integrated area, collected over the delayed fluorescence region (TD = 5 μs and Ti = 50 μs), was analyzed as a function of the laser excitation (337 nm) dose (Figure 4d). The intensity dependence shows a slope of 1.33 ± 0.03 at low excitation dose (<11 μJ), which turns to a linear dependence with slope of 1.00 ± 0.02 at high excitation doses. This suggests that the delayed fluorescence of this blend has a contribution of TTA, but it is not pure; otherwise, the behavior at low excitation doses would show a slope much closer to 2. Most probably, the TTA mechanism is not a pure process because the excitons in ^{3}LE need to collide with excitons in other **A**/**D** molecules to up convert them to ^{1}LE state, which is a slow process due to the bimolecular character. Therefore, we can deduce from the power dependence of the DF that there must also be a contribution coming from TADF as well. Thus, the delayed fluorescence mechanism in TPD:OXD-7 is most probably a mixture of TADF and TTA.

In summary, *m*-MTDATA:TPBi blend shows two energy splitting between ^{1}CT and ^{3}LE for the donor and acceptor molecules of ΔE_{ST} = (−0.01 ± 0.03) eV and ΔE_{ST} = (−0.02 ± 0.03) eV, respectively, which are very small, giving rise to TADF mechanism. TPD:TPBi blend shows the values of ΔE_{ST} = (0.61 ± 0.03) eV and ΔE_{ST} = (0.39 ± 0.03) eV, which TTA dominates because the triplet states are far below the ^{1}CT state. TPD:OXD-7 blend shows ΔE_{ST} = (0.51 ± 0.03) eV and ΔE_{ST} = (0.23 ± 0.03) eV, respectively. The results for this blend show that the DF mechanism is mixed TTA and TADF because one energy splitting favors TADF and the other favors TTA.

After analyzing the delayed fluorescence mechanisms in the different exciplex blends chosen systematically, we derived a collective energy diagram showing the full decay pathways available in these systems (Figure 5). Green dashed arrows represent the internal nonradiative transitions and green full ones represent the radiative transitions, which were detected by time dependence spectroscopy. Upon optical excitation of the donor or acceptor molecule, a population of CT states is formed, relatively slowly, $K_{ET} \approx 10^8$ s^{-1}, by electron or hole transfer. At early times, we detect the transitions ^{1}CT → S$_0$ and ^{1}LE$_D$ →S$_0$. Because the acceptor molecules studied absorb very weakly at 355 nm, the transition ^{1}LE$_A$ →S$_0$ is not detected. It is also highly likely that internal nonradiative transitions ^{1}LE$_A$ →^{1}LE$_D$ will occur as potentially would ^{1}LE$_A$ → ^{1}CT. Because ISC between ^{1}CT and ^{3}CT states potentially can only occur by hyperfine coupling (HFC) if the energy difference between the singlet and triplet CT states is very small, on the order of 10^{-3} meV, that is, when the electronic coupling between ^{1}CT ↔ ^{3}CT is effectively zero, this channel is extremely inefficient compared with that between the ^{1}CT state and a local excited

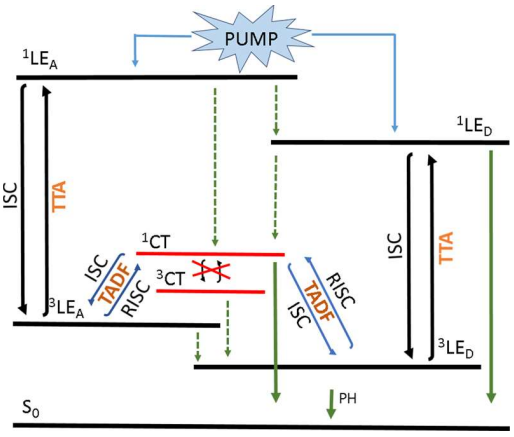

Figure 5. Energy diagram showing all radiative and nonradiative available pathways of decay in an exciplex blend.

triplet state (^{3}LE).[10] Therefore, the transition ^{1}CT ↔ ^{3}CT was assigned as a forbidden process in the diagram. The energy splitting between ^{1}CT ↔ ^{3}LE$_D$ and ^{1}CT ↔ ^{3}LE$_A$ depends on which molecules are chosen as donor and acceptor. If these energy splittings are small, excitons in the localized triplet levels gain enough thermal energy to match the ^{1}CT level and then cross, considering that rISC/ISC processes are adiabatic transitions. Hence, the transition ^{1}CT → S$_0$ is also detected at longer times and assigned as delayed fluorescence emission. If, however, these energy splittings are large, this mechanism is unlikely to occur. In this case another delayed fluorescence mechanism, TTA, which occurs between ^{1}LE$_A$ ↔ ^{3}LE$_A$, ^{1}LE$_D$ ↔ ^{3}LE$_D$, or ^{3}LE$_A$ ↔ ^{1}LE$_D$, converts two triplet excitons into one singlet exciton in ^{1}LE state and one in the ground state. If TTA occurs in the acceptor molecules, then the exciton converted to ^{1}LE$_A$ can go back to ^{3}LE$_A$ or compete with the transitions ^{1}LE$_A$ →^{1}LE$_D$ and ^{1}LE$_A$ →^{1}CT. Finally, at very late times and at low temperature, we detect the emission from the transition ^{3}LE$_D$ →S$_0$, phosphorescence. The transition ^{3}LE$_A$ → S$_0$ is not detected because the Dexter energy transfer from ^{3}LE$_A$ to ^{3}LE$_D$ may occur.

From power dependencies it is clear that TADF and TTA compete with each other. In the case when the singlet triplet gap between ^{1}CT and ^{3}LE is small and also one triplet state is not far below the ^{1}CT state, we see that TADF dominates. In all three cases the **D A** separation must be about the same at around 3 to 4 nm, and thus the ^{1}CT ^{3}CT separation would be expected to be very small in all cases. Thus, we can see, as with the case of ICT D−A molecules, that it is the LE CT gap that controls rISC and thus TADF efficiency in exciplexes as it does in the ICT molecules.[15,16]

These findings are essential for the design of exciplex blends. This means, to produce an exciplex blend showing efficient TADF, it is crucial to analyze the position of ^{3}LE of the donor and acceptor molecules with respect to the ^{1}CT emission. To date, the exciplex blends were designed to have the ^{1}CT state close to ^{3}CT, which can lie below both ^{3}LE$_D$ and ^{3}LE$_A$, but we show that this is not the energy splitting that should be considered. Also, we show that to achieve pure TADF both ^{3}LE states should be very close in energy to ^{1}CT, or at least one very close lying and one above ^{1}CT.

In our attempts to fully elucidate the underlying mechanism of exciplex systems, a set of 17 blends that show clear exciplex formation (emission) was selected and correlation with their

DOI: 10.1021/acs.jpcc.6b05198
J. Phys. Chem. C XXXX, XXX, XXX−XXX

Table 1. Energy Levels of Different Blends That Show Exciplex Formation[a]

material	HOMO (eV)	LUMO (eV)	H−H (eV)	L−L (eV)	^{1}CT onset (±0.02 eV)	triplet onset (±0.02 eV)	ΔE_{ST} (±0.03 eV)
m-MTDATA	5.1	2.0	−1.2	−0.8	2.64	2.65	−0.01
TPBi	6.3	2.8			2.64	2.66	−0.02
TPD	5.3	2.2	−1.0	−0.6	3.05	2.44	0.61
TPBi	6.3	2.8			3.05	2.66	0.39
TPD	5.3	2.2	−1.2	−0.6	2.95	2.44	0.51
OXD-7	6.5	2.8			2.95	2.72	0.23
TPD	5.3	2.2	−0.8	−0.6	3.06	2.44	0.62
BCP	6.1	2.8			3.06	2.56	0.50
TCTA	5.7	2.3	−0.8	−0.5	3.10	2.93	0.17
OXD-7	6.5	2.8			3.10	2.72	0.38
TCTA	5.7	2.3	−0.4	−0.5	3.24	2.93	0.31
BCP	6.1	2.8			3.24	2.56	0.68
TCTA	5.7	2.3	−0.6	−0.5	3.08	2.93	0.15
TPBi	6.3	2.8			3.08	2.66	0.42
TAPC	5.5	2.0	−0.6	−0.5	3.04	2.85	0.19
PBD	6.1	2.5			3.04	2.60	0.44
TAPC	5.5	2.0	−0.8	−0.8	3.13	2.85	0.28
TPBi	6.3	2.8			3.13	2.66	0.47
TAPC	5.5	2.0	−1.0	−0.8	3.07	2.85	0.22
OXD-7	6.5	2.8			3.07	2.72	0.35
m-MTDATA	5.1	2.0	−1.0	−0.5	2.62	2.65	−0.03
PBD	6.1	2.5			2.62	2.60	0.02
m-MTDATA	5.1	2.0	−1.4	−0.8	2.62	2.65	−0.03
OXD-7	6.5	2.8			2.62	2.72	−0.10
m-MTDATA	5.1	2.0	−1.0	−0.8	2.71	2.65	0.06
BCP	6.1	2.8			2.71	2.56	0.15
mCP	6.1	2.4	−0.4	−0.4	3.44	2.87	0.57
OXD-7	6.5	2.8			3.44	2.72	0.72
TAPC	5.5	2.0	−0.5	−1.0	2.78	2.85	−0.07
DPTPCz	6.0	3.0			2.78	2.91	−0.13
TCTA	5.7	2.3	−0.3	−0.7	2.81	2.93	−0.12
DPTPCz	6.0	3.0			2.81	2.91	−0.10
NPB	5.4	2.8	−0.6	−0.2	2.95	2.40	0.55
DPTPCz	6.0	3.0			2.95	2.91	0.04

[a]Energy values labeled as L−L in the Table are the energy differences between the LUMO of the donor and acceptor molecules. The same analyses were carried out for the HOMO energy levels.

HOMO/LUMO energy levels as well as their ^{1}CT/^{3}LE energy levels (Table 1). The HOMO/LUMO energy levels for the individual donor and acceptor molecules were taken from literature and used as an estimation because these values are sensitive to experimental conditions and vary considerably in the literature.[4,26−29] The ^{3}LE onset values of TCTA, mCP, and NPB also were taken from literature from phosphorescence spectra;[4,30,31] the other ^{3}LE spectra are in Figure S4. ^{1}CT onset values of the first 13 blends were taken from PL spectra from our experiments (Figure S5), and ^{1}CT onset values of the last 3 blends were estimated from PL spectra from ref 4. The energy values labeled as L−L in the table are the energy differences between the LUMO of the donor and acceptor molecules. The same analyses was carried out for the HOMO energy levels.

There is no obvious correlation among L−L or H−H values and exciplex formation (evidenced by CT emission); the exciplex is formed for low- and high-energy offset values. These values may influence the efficiency of charge transferred from donor to acceptor molecules, that is, the charge-transfer rates, but certainly the exciplex formation can occur for a large range of distinctive values of H−H and L−L. By the analyses of ΔE_{ST}, that is, the difference between ^{1}CT and ^{3}LE, it is possible to estimate which pairs of molecules are likely to yield a TADF mechanism. The negative values mean that the ^{3}LE is located above the ^{1}CT, a preferable characteristic for designing of efficient exciplex emitters because it prevents quenching of the excited states to a low-lying local triplet state, as previously reported,[9] but it is not essential for TADF to occur. *m*-MTDATA:PBD blend shows both ΔE_{ST} values to be very small, very promising for the TADF mechanism. This blend was demonstrated to have strong TADF,[2,32] and our analysis provides a better understanding of the good performance of its TADF mechanism. *m*-MTDATA:OXD-7 also shows both ΔE_{ST} values likely for TADF, which was also confirmed by time-resolved optical spectroscopy (Figure S6). TPD:BCP blend shows both ΔE_{ST} values large, which have the TTA mechanism confirmed by time-resolved optical spectroscopy (Figure S7). TAPC:PBD shows energy splitting values close to those of TPD:OXD-7, one ΔE_{ST} likely for TADF and another for TTA. The mix of the delayed fluorescence mechanisms was confirmed in this blend (Figure S8). Chen et al. have compared the performance of the OLEDs produced with emissive layers of *m*-MTDATA:TPBi and *m*-MTDATA:BCP, with measurements carried out under the same conditions.[33] The first one has shown better performance, which was associated with the largest exciplex bandgap (energy difference between the

DOI: 10.1021/acs.jpcc.6b05198
J. Phys. Chem. C XXXX, XXX, XXX−XXX

LUMO of the donor and the HOMO of the acceptor). By our analyses, it is possible to associate the better performance of *m*-MTDATA:TPBi with the smaller values of both ΔE_{ST}. These smaller energy values lead to a stronger TADF characteristic and consequently a better performance if compared with *m*-MTDATA:BCP device. Liu et al.[4] have compared three exciplex blends, TAPC:DPTPCz, TCTA:DPTPCz, and NPB:DPTPCz. The TADF mechanism was identified in the first two blends. These results are in agreement with our analyses because TAPC:DPTPCz and TCTA:DPTPCz blends have ^{1}CT and ^{3}LE very close in energy; on the contrary, NPB:DPTPCz blend shows one ^{3}LE level located far below the ^{1}CT, preventing efficient rISC.

Understanding comes from the observation of mixed TADF and TTA, as found in many systems. The cases where TADF dominates are rare and correlate to the absence of a low-lying quenching local triplet state. However, in all cases showing at least a contribution of TADF, an ^{3}LE states lies very close in energy to ^{1}CT, even if the other ^{3}LE state lies well below the CT states, causing quenching. The rISC rates depend on energy gap and electronic coupling, and thus only in special cases will the "pure" TADF be observed; this will be a very resonant effect. Hence, we only (partially) observe mono-exponential decay from ^{1}CT showing a unique species in *m*-MTDATA:TPBi. If the ^{1}CT and ^{3}CT orbitals were not very close to degenerate, then the exchange energy would be large, that is, bigger than 50−100 meV. This might "allow" some direct SOC between them, but then the gap between ^{1}CT and ^{3}CT would be too large to yield efficient TADF, and we clearly observe TADF. The clear observation of TADF indicates that ^{1}CT, ^{3}CT, and ^{3}LE are *all* near-isoenergetic allowing efficient TADF and no quenching to a low-lying triplet state yielding TTA. However, when mixed TADF and TTA is observed, the case when ^{1}CT, ^{3}CT, and ^{3}LE are *all* near isoenergetic but the other local triplet lies below them, then a competition between rISC and ^{1}CT emission with quenching to the low-lying ^{3}LE state has to be fairly equal such that both mechanisms compete. A low-lying local triplet state does not always lead to full quenching of TADF.

CONCLUSIONS

Three blends made of well-known electron donor and acceptor materials (*m*-MTDATA:TPBi, TPD:OXD-7, and TPD:OXD-7) were studied by time-dependent spectroscopy. It is shown that the ISC/rISC processes between ^{1}CT and ^{3}CT are mediated by a local triplet state (^{3}LE) following a similar mechanism recently shown for ICT TADF molecules. Consequently, to obtain TADF emission, a ^{3}LE state from the donor or acceptor molecules must be close enough in energy to the CT states to minimize the thermal activation barrier, that is, achieving vibronic coupling between ^{3}LE and ^{3}CT. However, for many systems (studied here as well as taken from the literature), mixed TADF and TTA is observed. By analyzing the competition between TTA and TADF we find that for those systems with an energetically close-lying ^{1}CT and ^{3}LE the TADF mechanism dominates; in contrast, TTA dominates for larger ΔE_{ST} because the residence time in the triplet state is long and TTA outcompetes rISC. In the case of one close-lying and one lower energy LE state, mixed TTA and TADF can be observed showing that the two processes compete fairly equally. In the case the low-lying ^{3}LE state does not completely quench the TADF. Moreover, we analyze the role of the highest occupied and lowest unoccupied molecular orbital (HOMO/LUMO) energy levels between the electron donor and acceptor molecules in the exciplex formation by combining the results of a vast number of exciplex systems, showing no obvious correlation between energy offset and TADF to these values because the ^{1}CT and ^{3}LE energy difference dominates this property. Our studies thus open a new development route for the design of new material selection for delayed fluorescence device based on TADF mechanism.

ASSOCIATED CONTENT

Supporting Information

The Supporting Information is available free of charge on the ACS Publications website at DOI: 10.1021/acs.jpcc.6b05198.

Complementary optical spectroscopy−steady state and time-resolved spectra. (PDF)

AUTHOR INFORMATION

Corresponding Author

*E-mail: a.p.monkman@durham.ac.uk. Tel: +44 (0) 191 3343616.

Author Contributions

P.L.d.S. performed the experimental work and analyzed the data. P.L.d.S. wrote the manuscript with contributions from A.P.M. and F.B.D. All authors determined the phenomenology of the results.

Notes

The authors declare no competing financial interest.

ACKNOWLEDGMENTS

P. L. dos Santos thanks CAPES Foundation, Ministry of Education of Brazil, Brasilia - DF 70040-020, Brazil, in particular. the Science Without Borders Program for a Ph.D. studentship, Proc. 12027/13-8. All authors acknowledge EPSRC grant EP/K016164/1.

REFERENCES

(1) Hung, W.; Fang, G.; Chang, Y.; Kuo, T.; Chou, P.; Lin, S.; Wong, K. Highly Efficient Bilayer Interface Exciplex For Yellow Organic Light- Emitting Diode. *ACS Appl. Mater. Interfaces* **2013**, *5*, 6826−6831.

(2) Graves, D.; Jankus, V.; Dias, F. B.; Monkman, A. Photophysical Investigation of the Thermally Activated Delayed Emission from Films of M-MTDATA: PBD Exciplex. *Adv. Funct. Mater.* **2014**, *24*, 2343−2351.

(3) Zhang, T.; Zhao, B.; Chu, B.; Li, W.; Su, Z.; Wang, L.; Wang, J.; Jin, F.; Yan, X.; Gao, Y.; et al. Blue Exciplex Emission and Its Role as a Host of Phosphorescent Emitter. *Org. Electron.* **2015**, *24*, 1−6.

(4) Liu, X.-K.; Chen, Z.; Zheng, C.-J.; Liu, C.-L.; Lee, C.-S.; Li, F.; Ou, X.-M.; Zhang, X.-H. Prediction and Design of Efficient Exciplex Emitters for High-Efficiency, Thermally Activated Delayed-Fluorescence Organic Light-Emitting Diodes. *Adv. Mater.* **2015**, *27*, 2378−2383.

(5) Chen, B.; Zhang, X. H.; Lin, X. Q.; Kwong, H. L.; Wong, N. B.; Lee, C. S.; Gambling, W. A.; Lee, S. T. Improved Color Purity and Efficiency of Blue Organic Light-Emitting Diodes via Suppression of Exciplex Formation. *Synth. Met.* **2001**, *118*, 193−196.

(6) Chan, L. H.; Lee, R. H.; Hsieh, C. F.; Yeh, H. C.; Chen, C. T. Optimization of High-Performance Blue Organic Light-Emitting Diodes Containing Tetraphenylsilane Molecular Glass Materials. *J. Am. Chem. Soc.* **2002**, *124* (22), 6469−6479.

(7) Dias, F. B.; Bourdakos, K. N.; Jankus, V.; Moss, K. C.; Kamtekar, K. T.; Bhalla, V.; Santos, J.; Bryce, M. R.; Monkman, A. P. Triplet Harvesting with 100% Efficiency by Way of Thermally Activated

DOI: 10.1021/acs.jpcc.6b05198
J. Phys. Chem. C XXXX, XXX, XXX−XXX

Delayed Fluorescence in Charge Transfer OLED Emitters. *Adv. Mater.* **2013**, *25*, 3707−3714.
(8) Weller, H. B.; A. Characteristics of Molecular Complexes in the Excited State. *Acta Phys. Pol.* **1968**, *34*, 593−542.
(9) Jankus, V.; Chiang, C. J.; Dias, F.; Monkman, A. P. Deep Blue Exciplex Organic Light-Emitting Diodes with Enhanced Efficiency; P-Type or E-Type Triplet Conversion to Singlet Excitons? *Adv. Mater.* **2013**, *25*, 1455−1459.
(10) Lim, B. T.; Okajima, S.; Chandra, A. K.; Lim, E. C. Radiationless Transitions in Electron Donor-Acceptor Complexes: Selection Rules for S1 → T Intersystem Crossing and Efficiency of S1 → S0 Internal Conversion. *Chem. Phys. Lett.* **1981**, *79*, 22−27.
(11) Dance, Z. E. X.; Mickley, S. M.; Wilson, T. M.; Ricks, A. B.; Scott, A. M.; Ratner, M. A.; Wasielewski, M. R. Intersystem Crossing Mediated by Photoinduced Intramolecular Charge Transfer: Julolidine-Anthracene Molecules with Perpendicular Pi Systems. *J. Phys. Chem. A* **2008**, *112* (18), 4194−4201.
(12) Marian, C. M. On the Mechanism of the Triplet-to-Singlet Upconversion in the Assistant Dopant ACRXTN. *J. Phys. Chem. C* **2016**, *120*, 3715−3721.
(13) Chen, X.-K.; Zhang, S.-F.; Fan, J.-X.; Ren, A.-M. Nature of Highly Efficient Thermally Activated Delayed Fluorescence in OLED Emitters: Non-Adiabatic Effect Between Excited States. *J. Phys. Chem. C* **2015**, *119*, 9728−9733.
(14) Gibson, J.; Monkman, A.; Penfold, T. J. The Importance of Vibronic Coupling for Efficient Reverse Intersystem Crossing. *ChemPhysChem***2016**, 10.1002/cphc.201600662.
(15) Santos, P. L.; Ward, J. S.; Data, P.; Batsanov, A. S.; Bryce, M. R.; Dias, F. B.; Monkman, A. P. Engineering the Singlet−triplet Energy Splitting in a TADF Molecule. *J. Mater. Chem. C* **2016**, *4*, 3815−3824.
(16) Data, P.; Pander, P.; Okazaki, M.; Takeda, Y.; Minakata, S.; Monkman, A. P. Dibenzo[a,j]phenazine-Cored Donor−Acceptor−Donor Compounds as Green-to-Red/NIR Thermally Activated Delayed Fluorescence Organic Light Emitters. *Angew. Chem., Int. Ed.* **2016**, *55*, 5739.
(17) Marian, C. M. Spin-Orbit Coupling and Intersystem Crossing in Molecules. *Wiley Interdiscip. Rev. Comput. Mol. Sci.* **2012**, *2*, 187−203.
(18) Masmanidis, C. A.; Jaffe, H. H.; Ellis, R. L. Spin-Orbit Coupling in Organic Molecules. *J. Phys. Chem.* **1975**, *79*, 2052−2061.
(19) Turro, N. J. *Modern Molecular Photochemistry*; The Benjamin/Cummings Publishing Company: Menlo Park, CA, 1978
(20) Al Attar, H. A.; Monkman, A. P. Electric Field Induce Blue Shift and Intensity Enhancement in 2D Exciplex Organic Light Emitting Diodes; Controlling Electron-Hole Separation. *Adv. Mater.* **2016**, DOI: 10.1002/adma.201600965.
(21) Imaizumi, K.; Mori, T.; Mizutani, T. Injection and Transport of Carriers at Organic Interfaces in Organic Light-Emitting-Diode with Oxadiazole Derivatives. *IEEE 1997 Annu. Rep. Conf. Electr. Insul. Dielectr. Phenom.* **1997**, *2*, 459−462.
(22) Haverinen, H. M.; Myllylä, R. A.; Jabbour, G. E. Inkjet Printing of Light Emitting Quantum Dots. *Appl. Phys. Lett.* **2009**, *94*, 073108−1.
(23) Zhang, G.; Li, W.; Chu, B.; Su, Z.; Yang, D.; Yan, F.; Chen, Y.; Zhang, D.; Han, L.; Wang, J.; et al. Highly Efficient Photovoltaic Diode Based Organic Ultraviolet Photodetector and the Strong Electroluminescence Resulting from Pure Exciplex Emission. *Org. Electron.* **2009**, *10*, 352−356.
(24) Chen, S.; Wu, Z.; Zhao, Y.; Li, C.; Hou, J.; Liu, S. Efficient Organic Light-Emitting Device from Exciplex Emission between 4,4̀,4̀-tris[3-Methylphenyl(phenyl)amino]triphenylamine and 2,2̀,2̀-(1,3,5-Benzenetriyl)tris-[1-Phenyl-1H-Benzimidazole]. *Org. Electron.* **2005**, *6*, 111−117.
(25) Dias, F. B. Kinetics of Thermal-Assisted Delayed Fluorescence in Blue Organic Emitters with Large Singlet − Triplet Energy Gap. *R. Soc., A* **2015**, *373*, 20140447.
(26) Etori, H.; Yasuda, T.; Jin, X. L.; Fujita, K.; Mataka, S.; Tsutsui, T. Design of Multilayer Structure for UV Organic Light-Emitting Diodes Based on 2-(2-Naphthyl)-9,9-Spirobifluorene. *Japanese J. Appl. Physics* **2007**, *46*, 5071−5075.
(27) Jeon, S. O.; Yook, K. S.; Joo, C. W.; Lee, J. Y. A Phosphine Oxide Derivative as a Universal Electron Transport Material for Organic Light-Emitting Diodes. *J. Mater. Chem.* **2009**, *19*, 5940−5944.
(28) Mohd Sarjidan, M. A.; Za'aba, N. K.; Basri, S. H.; Zaini, S. N.; Zaini, M. S.; Abd Majid, W. H. Blending Effect on Small Molecule Based OLED. *Optoelectron. Adv. Mater. Rapid Commun.* **2013**, *7*, 498−501.
(29) Yang, Y.; Cohn, P.; Dyer, A. L.; Eom, S. H.; Reynolds, J. R.; Castellano, R. K.; Xue, J. Blue-Violet Electroluminescence from a Highly Fluorescent Purine. *Chem. Mater.* **2010**, *22*, 3580−3582.
(30) Kim, J. W.; You, S. I.; Kim, N. H.; Yoon, J.-A.; Cheah, K. W.; Zhu, F. R.; Kim, W. Y. Study of Sequential Dexter Energy Transfer in High Efficient Phosphorescent White Organic Light-Emitting Diodes with Single Emissive Layer. *Sci. Rep.* **2014**, *4*, 7009.
(31) Reineke, S.; Lindner, F.; Schwartz, G.; Seidler, N.; Walzer, K.; Lüssem, B.; Leo, K. White Organic Light-Emitting Diodes with Fluorescent Tube Efficiency. *Nature* **2009**, *459*, 234−238.
(32) Goushi, K.; Yoshida, K.; Sato, K.; Adachi, C. Organic Light-Emitting Diodes Employing Efficient Reverse Intersystem Crossing for Triplet-to-Singlet State Conversion. *Nat. Photonics* **2012**, *6*, 253−258.
(33) Chen, P.; Peng, Q.; Yao, L.; Gao, N.; Li, F. Identifying the Efficient Inter-Conversion between Singlet and Triplet Charge-Transfer States by Magneto-Electroluminescence Study. *Appl. Phys. Lett.* **2013**, *102*, 063301.

DOI: 10.1021/acs.jpcc.6b05198
J. Phys. Chem. C XXXX, XXX, XXX−XXX